Behavior of Evaporating Droplets at Nonsoluble and Soluble Surfaces: Modeling with Molecular Resolution

Rodrigo M. Cordeiro and Tadeusz Pakula*

Max Planck Institute for Polymer Research, Ackermannweg 10, D-55128 Mainz, Germany

Liquid droplets in equilibrium with vapor are simulated at solidlike surfaces using the *cooperative motion algorithm* (CMA). These droplets behave like real droplets, i.e., the densities of the coexistent liquid and vapor phases obey empirical relations such as $\rho_l - \rho_v \propto (1 - T/T_c)^{1/3}$. Droplet evaporation was studied under various interaction conditions, i.e., nonsoluble and soluble substrates. In the last case, substrate particles migrate toward the liquid−vapor interface to minimize the droplet surface energy. This leads to the formation of a microwell surrounded by a ringlike deposit on the substrate surface. It is shown that the ring formation in the first stages of evaporation results in pinning of the droplet contact area.

1. Introduction

Surface microstructuring is a field of interest to both basic research and industrial applications. The most appealing surface patterning techniques are those that are experimentally simple and enable the control of the pattern shape. It was recently shown that it is possible to create microwells by bringing solvent drops onto a soluble polymer substrate.[1,2] The process is analogous to the formation of ringlike deposits when, for example, a coffee drop evaporates and leaves a ring shaped stain of solid particles on the substrate.[3,4] The difference is that, in the first case, the solid left by the droplet was not initially dissolved in it, but is gradually dissolved from the substrate as the droplet evaporates. The effect is very general, i.e., it can be observed for a large variety of substances. As the droplet evaporates, the substrate material is removed from the center and deposited on the border of the droplet contact area. This process generates a microwell surrounded by a ringlike deposit, as shown in Figure 1. The microwell can be used, for example, as a chemical microreactor or as a mask for molding of microlenses.[1]

A phenomenological model to explain the ringlike deposit formation is already available in the literature. In this model, the contact area between droplet and substrate is considered to be pinned. As the liquid evaporates, an outward liquid flux is considered as necessary to compensate for the amount of liquid that evaporated from the border (Figure 2). This flux is responsible for the transportation of dissolved material to the border, where it is concentrated and finally precipitates.[1,3,4] Although the model accounts very well for microwell and ringlike deposit formation, it cannot clarify the role of molecular interactions involved in this process. Furthermore, it is still not clear if the pinning of the contact area is really a requirement for the ring formation or if it is instead a consequence of the ring formation. These questions are also very difficult to be clarified experimentally.

Therefore, to investigate microwell and ringlike deposit formation with a molecular approach, we performed in-lattice Monte Carlo simulations of liquid droplets on surfaces and in equilibrium with a vapor phase. The method used was the so-
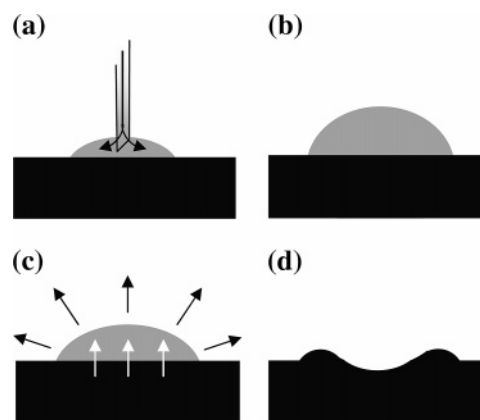
* Author to whom correspondence should be addressed. Phone: +49-6131-379113. Fax: +49-6131-379100. E-mail: pakula@mpip-mainz.mpg.de.

Figure 1. Different stages of microwell and ringlike deposit formation. (a) Solvent is placed on a soluble surface with a syringe. (b) A droplet is formed. (c) Substrate is slowly dissolved (white arrows) while the droplet evaporates (black arrows). (d) A microstructure is left on the surface.
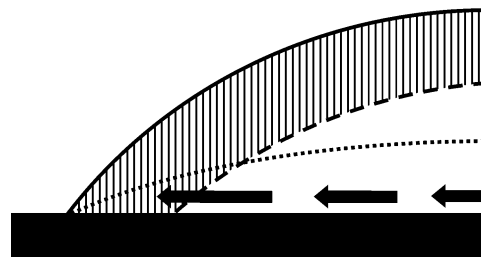

Figure 2. Evaporation dynamics of nonpinned (- - -) and pinned (···) droplets. Full line represents the initial shape of the droplet, and the shaded area is the amount of evaporated solvent. The arrows indicate the compensating liquid flux that keeps the contact line fixed when the droplet is pinned.

called *cooperative motion algorithm* (CMA), which has been successfully applied in the simulation of lattice liquids and polymer melts.[5,6] This method is highly efficient and can be easily implemented in a common personal computer (PC). Another advantage is that intermolecular interactions are adjustable parameters in this algorithm.

The first part of this paper is dedicated to a brief description of the CMA principles and its application in the simulation of liquid droplets. We shall demonstrate that the simulated droplets reproduce satisfactorily the behavior of real droplets whose size

Modeling of Evaporating Droplets at Surfaces

J. Phys. Chem. B, Vol. 109, No. 9, 2005 **4153**

TABLE 1: Average Quantities Obtained from the Simulations (Error Is in the Last Digit)

kT	system feature[a]	size[b]	solvent amount	ρ_l	ρ_v	ξ_l	ξ_v	R_e	D
2.0	drop on surface	9.6×10^4	1.35×10^4	0.998	0.0017	0.014	0.020	29.0	3.37
2.8	drop on surface	9.6×10^4	1.35×10^4	0.990	0.0117	0.1192	0.0365	29.4	4.23
3.0	drop on surface	9.6×10^4	1.35×10^4	0.9856	0.0163	0.168	0.1896	29.07	3.47
3.0	drop on surface	2.5×10^5	1.35×10^4	0.9857	0.01619	0.166	0.188	26.2	3.75
3.0	free drop	2.5×10^5	1.35×10^4	0.9864	0.0184	0.157	0.213	15.8	3.18
3.0	free drop	2.5×10^5	7.2×10^3	0.9876	0.0187	0.142	0.217	12	2.44
3.0	film	2.5×10^5	7.5×10^4	0.9845	0.0156	0.1811	0.182		2.78
3.5	drop on surface	2.5×10^5	1.35×10^4	0.9712	0.0333	0.324	0.3767	23.5	6.01
4.0	drop on surface	9.6×10^4	1.35×10^4	0.945	0.0589	0.593	0.635	29.74	6.71
4.0	free drop	6.25×10^4	1.35×10^4	0.947	0.0634	0.572	0.678	16	6.22
4.0	film	9.6×10^4	4.8×10^4	0.9432	0.0568	0.618	0.617		3.99
4.3	drop on surface	9.6×10^4	1.35×10^4	0.922	0.0805	0.781	0.8367	30.97	7.5
5.0	film	9.6×10^4	4.8×10^4	0.841	0.157	1.442	1.42		7.34

[a] In all cases, the interaction energies of SO−VA, SO−SU, and SU−VA were 1, 0.5, and 1, respectively. [b] The system size is regarded as the sum of solvent and vacuum beads. Substrate beads are not counted because their motion is forbidden.

is on the order of nanometers, but the same results can be extended to micrometer-sized droplets. In the last part, the method will be applied to simulate the microwell and ringlike deposit formed when a droplet evaporates on the surface of a soluble substrate. It turns out that an appropriate choice of the interaction parameters is crucial for microstructure formation and that analysis of molecular interactions provides information relevant for both basic understanding and technological application of this effect.

2. Simulation Method

The cooperative motion algorithm (CMA) used in this work has already been successfully applied in the simulation of dense systems such as lattice liquids and polymer melts.[5,6] In this model, an ensemble of beads is created on a tridimensional lattice (face-centered cubic) that serves as a coordination skeleton. Each lattice site is occupied by a single bead representing, for instance, a molecular element or a molecular aggregate. There is no empty site in the lattice, and two beads cannot occupy simultaneously the same position. The program simulates the collective motion of beads along closed random loops. Each element replaces one of its neighbors, and the sum of all displacements is zero.

In this work, the beads on the lattice are regarded as having three types of identity. They are labeled to represent either solvent particles (SO), substrate particles (SU), or vacuum (VA). Although the beads can exchange places with each other, their identity is conserved. The repulsive energy of interaction between two neighboring beads is considered as zero if they have the same identity and as a finite and positive number if they have different identities. Before each movement, the probability of acceptance of a bead in the next position is calculated. At a given temperature, this probability is given by the Boltzmann factor[5]

$$p = e^{-E/kT} \tag{1}$$

where E is the energy of interaction of the moving bead with neighbors in the next position, given by

$$E_i = n_{ij}\epsilon_{ij} + n_{ik}\epsilon_{ik} \tag{2}$$

in which ϵ represents the interaction energy between two beads and n the number of interactions. The different subscripts indicate that only interactions between beads with different identity contribute to the total energy. Both E and kT are considered in arbitrary units. The factor p is compared to a random number from 0 to 1 generated by the computer. Every time p is higher than the random number, the movement is performed; otherwise the program will search for another

position to move the bead. The final system generated in this way can be regarded as being in equilibrium at a chosen temperature (kT).

The consequence of all of these assumptions is that during the system equilibration beads of the same identity tend to aggregate since the intermixing of phases costs energy. As will be shown, solvent beads tend to aggregate in a spherical-shaped phase to minimize their contact with vacuum, i.e., they form a droplet.

Simulations of droplets on surfaces, free-standing droplets, and liquid films on surfaces were performed. Although our main interest was in droplets on surfaces, the other situations were important to show that the surface tension of the solvent in equilibrium with its vapor is the same in all the cases, as one would expect in reality.

In the simulations of droplets on surfaces, the initial system configuration was a cubic droplet of pure solvent placed upon a layer of substrate material and surrounded by vacuum. The simulation then started and proceeded until the cubic droplet had relaxed to a droplet with the shape of a spherical cap. During the relaxation of the cubic droplet, the motion of substrate beads was forbidden to avoid their intermixing with solvent or vacuum. However, substrate beads on the surface could still interact with solvent or vacuum, and the energies of interaction determined the substrate wettability. Periodic boundary conditions were applied only in the directions parallel to the substrate surface. A similar initial configuration was used in the simulations of free-standing droplets with the difference that the substrate was absent and all the boundaries were periodic. In the case of liquid films on a substrate, the initial system configuration was a layer of pure solvent between substrate and vacuum. As the simulation started, solvent and vacuum started to intermix.

Simulations were carried out for systems with different sizes, as shown in Table 1. The total number of beads in each system was on the order of 10^5. It is observed that the system size and the proportion between its components do not influence the thermodynamic properties of the droplets, as one would expect for real droplets. However, the appropriate choice of system size plays still a crucial role.[7] If the system volume is very large compared with the initial amount of liquid, then the solvent will evaporate at temperatures considerably lower than the critical temperature, and no droplet will be formed. In such a system, the solvent and vacuum beads are completely intermixed. Analogously, if the initial amount of solvent is too high, then the liquid phase can spread until it reaches the periodic boundaries. In this case, a solvent film will be formed instead of a droplet.

As the simulation starts, each movement attempt is considered as a Monte Carlo step, regardless of the identity of the moving
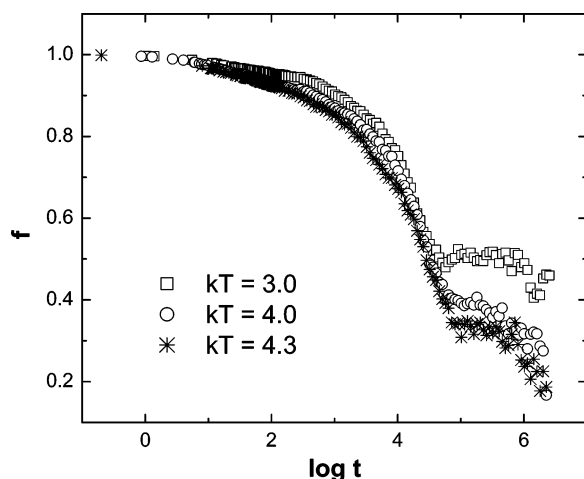
Figure 3. Shape correlation function for droplets on a surface at several temperatures. The interaction energies of SO−VA, SO−SU, and SU−VA were 1, 0.5, and 1, respectively.

bead or whether the attempted motion is successful or not. A unit of time is assumed to correspond to a number of attempts equal to the number of elements in the system. During one unit of time, the system performs on average one motion attempt per element. To evaluate the time necessary to drive the systems to the equilibrium condition, we defined a so-called "shape correlation function" *f* given by

$$f = \frac{1}{N_s} \sum_i a_i(0)a_i(t) \qquad (3)$$

where N_s is the total number of solvent beads and $a_i(t)$ defines the occupation of each lattice site *i* at a time *t*. If the lattice site is occupied by a solvent bead, then $a_i(t) = 1$; otherwise $a_i(t) = 0$. The shape correlation function measures which fraction of the sites that accommodated a solvent at $t = 0$ also accommodates a solvent at a time *t*. Figure 3 shows the typical behavior of *f* as a function of simulation time. As the droplet relaxes from a cube to its equilibrium shape, *f* decreases from 1 to a finite value. The intermixing between solvent and vacuum also contributes to the decrease of *f*. In times on the order of 10^5, the correlation function reaches a plateau, and the system can be considered to be fully relaxed. In all simulations, the systems were allowed to relax for a period at least 10 times longer than the time needed to reach the plateau. If droplets relax for very long times, then they can also move in relation to their initial position. Because of that, a further decrease in *f* after the plateau can be observed in some cases.

The droplets were allowed to relax under various conditions. The influence of parameters such as temperature and interaction between beads was systematically studied. After the relaxation, sampling started for the thermodynamic averages every ∼10^6 Monte Carlo steps. Average quantities such as the energy density in the liquid and vapor phases were calculated. We also calculated the occupancy of each lattice site, i.e., the fraction of time it is occupied by a solvent bead. This allowed determination of the average shape of the droplets, their radius of curvature, and their density profile across the interface. Generally, the time required to obtain smooth density profiles was equivalent to about 10 relaxation times.

All simulations were performed in common PCs. Due to the high efficiency of the method, large systems (∼10^5 elements) could be simulated within hours.
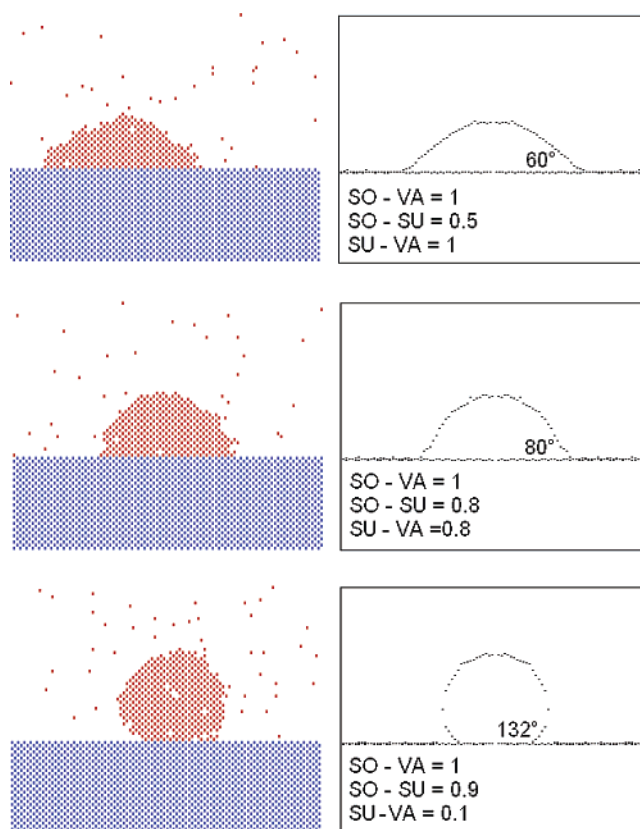

Figure 4. Different droplet shapes generated by varying the interaction energies between beads. Left pictures are snapshots of the system. Blue and red dots are substrate and solvent, respectively. Vacuum beads were not represented for simplicity. Right boxes are 360° radial averages of the corresponding snapshots. Points near the center of symmetry should be disregarded due to the small number of beads sampled in this region. The contact angles were obtained by fitting the shapes as spherical caps.

3. Results and Discussion

3.1. Validation of the Model. The validity of the model can be tested by analyzing how the droplet shape depends on the interaction energies between beads. As stated earlier, solvent beads tend to form an aggregated phase to minimize their contact area with vacuum. If there is no substrate, then the droplet will have the shape of a sphere. However, if a substrate is present, then three kinds of repulsive interactions should be considered, namely, SO−VA, SO−SU, and SU−VA. Figure 4 shows snapshots of droplets with different shapes. The SO−VA interaction was the same in all cases, but the other two were varied. If the repulsive interaction SO−SU is less than that of SU−VA, then the solvent wets the substrate, and the contact angle of the resulting droplet is lower than 90°. The opposite happens if the repulsive interaction of SO−SU is considered higher than that of SU−VA. In this case, the solvent hardly wets the substrate, and the contact angle is higher than 90°. These features are in qualitative agreement with experiments.

Another way to validate the model is to compare the thermodynamic properties of simulated droplets with those of real droplets. For that, quantities such as the surface energy and the densities of the liquid and vapor coexisting phases were calculated. The density was defined as the fraction of solvent beads in a given region of the lattice. Figure 5 shows typical density profiles recorded for simulated droplets. The density varies as a function of distance from the center of curvature of the droplets. It is initially constant and corresponds to the liquid-phase density. At a given distance, the density decreases to a lower plateau that corresponds to the density of the vapor. The
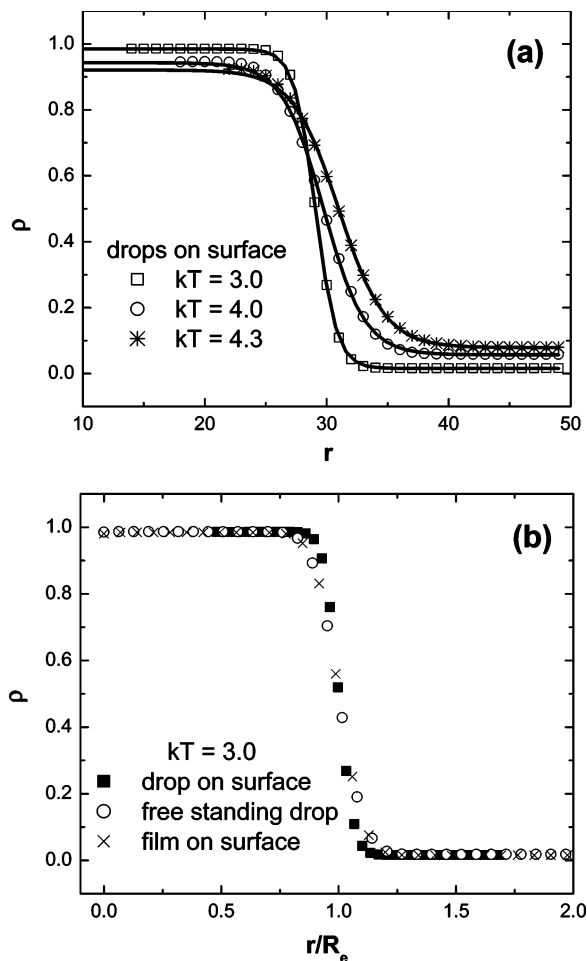
Modeling of Evaporating Droplets at Surfaces

J. Phys. Chem. B, Vol. 109, No. 9, 2005 **4155**

Figure 5. (a) Density as function of distance from the center of curvature for droplets on a surface at different temperatures (full lines represent the tanh fitting). (b) Density as function of distance (normalized to the equimolar dividing surface), showing that drops on surface, free drops, and films on a surface behave similarly.

transition between liquid and vapor is smooth, and the density profile can be fitted by a tanh function[7,8]

$$\rho(r) = \left(\frac{1}{2}\right)(\rho_l + \rho_v) - \left(\frac{1}{2}\right)(\rho_l - \rho_v)\tanh{(2(r - R_e)/D)} \quad (4)$$

where r is the distance from the droplet center of curvature, R_e is the radius of the equimolar dividing surface, and D is a parameter related to the interface thickness. The parameters obtained from the fitting procedure are depicted in Table 1.

It is well-known that when bulk liquids are in equilibrium with their vapor the following empirical relations hold for the density of the coexisting phases[9,10]

$$\frac{\rho_v}{\rho_c} = 1 + \frac{3}{4}\left(1 - \frac{T}{T_c}\right) - \frac{7}{4}\left(1 - \frac{T}{T_c}\right)^{1/3} \quad (5)$$

$$\frac{\rho_l}{\rho_c} = 1 + \frac{3}{4}\left(1 - \frac{T}{T_c}\right) + \frac{7}{4}\left(1 - \frac{T}{T_c}\right)^{1/3} \quad (6)$$

$$\frac{\rho_l - \rho_v}{\rho_c} = \frac{7}{2}\left(1 - \frac{T}{T_c}\right)^{1/3} \quad (7)$$

$$\frac{\rho_l + \rho_v}{2\rho_c} = 1 + \frac{3}{4}\left(1 - \frac{T}{T_c}\right) \quad (8)$$

where ρ represents the density of the liquid (l), the vapor (v), or at the critical point (c). According to eqs 5 and 6, the density

of the vapor increases as temperature increases, while the opposite happens with the density of the liquid. When the critical temperature is reached, the density of liquid and vapor are equal, and the system becomes monophasic, i.e., the boundary between liquid and vapor disappears. To test whether simulations reproduce this effect or not, droplets were simulated at various temperatures, and the densities of the coexisting phases were determined. Although temperature was varied, the interactions SO−VA, SO−SU, and SU−VA had fixed values of 1, 0.5, and 1, respectively. The liquid−vapor coexistence diagram constructed with the simulated densities is shown in Figure 6a. Droplets generated at temperatures lower than 2.8 are not considered here because they are not spherically shaped. They exhibit flat surfaces such as a crystal, and the system can be regarded as being a solid in equilibrium with vapor. Thus, the temperature of ~2.8 represents the triple point.

Above this temperature, the densities of the coexisting phases follow qualitatively the behavior previously described. The results do not depend on system size. Moreover, droplets on a surface, free-standing droplets, and liquid films on surface follow the same tendency. This is in accordance with experiment; since the density is an intrinsic property of the liquid, it does not matter if it is a droplet or a film.

Figure 6a shows that, by considering $\rho_c = 0.5$, it is possible to fit the part of the coexistence curve corresponding to vapor with $kT_c = 5.33 \pm 0.06$. However, the density of the liquid calculated by substituting these parameters in eq 6 does not agree with the values of ρ_l obtained from simulations. Such disagreement is due to the fact that the simulation does not account for the thermal expansion of the liquid phase. This problem can be solved by correcting the liquid phase densities as described in Appendix 1. In fact, Figure 6a shows that a fairly good agreement is observed between eq 6 and the simulated data after such a correction.

Through the use of the corrected values of the liquid density, a good agreement between data from simulation and eqs 7 and 8 is also observed in Figures 6b and 6c, respectively.

The difference between the densities of coexisting phases can be converted to the surface tension of the droplets. According to literature,[9,10] the temperature dependence of the surface tension of bulk liquids is given by the empirical equation

$$\gamma = \gamma_0(1 - T/T_c)^\alpha \quad (9)$$

where γ is the surface tension, γ_0 is the surface tension at zero temperature, and α is a parameter close to $^{11}/_9$ for simple liquids. For instance, a value of 1.302 ± 0.006 for α was reported for liquid Xenon.[11] The ratio γ/γ_0 can be determined by the combination of eqs 7 and 9 and considering $\alpha = {}^{11}/_9$, and its temperature dependence is shown in Figure 7a.

In this work, the parameter γ/γ_0 was determined indirectly by means of the densities. Direct determination of the surface tension by means of arguments involving the free energy of the system would be more complicated. In this case, one should count both enthalpic and entropic contributions. The calculation of the enthalpy alone, however, is a more straightforward procedure, since one only needs to count the strength of interaction in the system. More precisely, the surface enthalpy h can be determined by

$$hA = E_T - \xi_l V_l - \xi_v V_v \quad (10)$$

where A is the droplet surface area, E_T the total energy of the
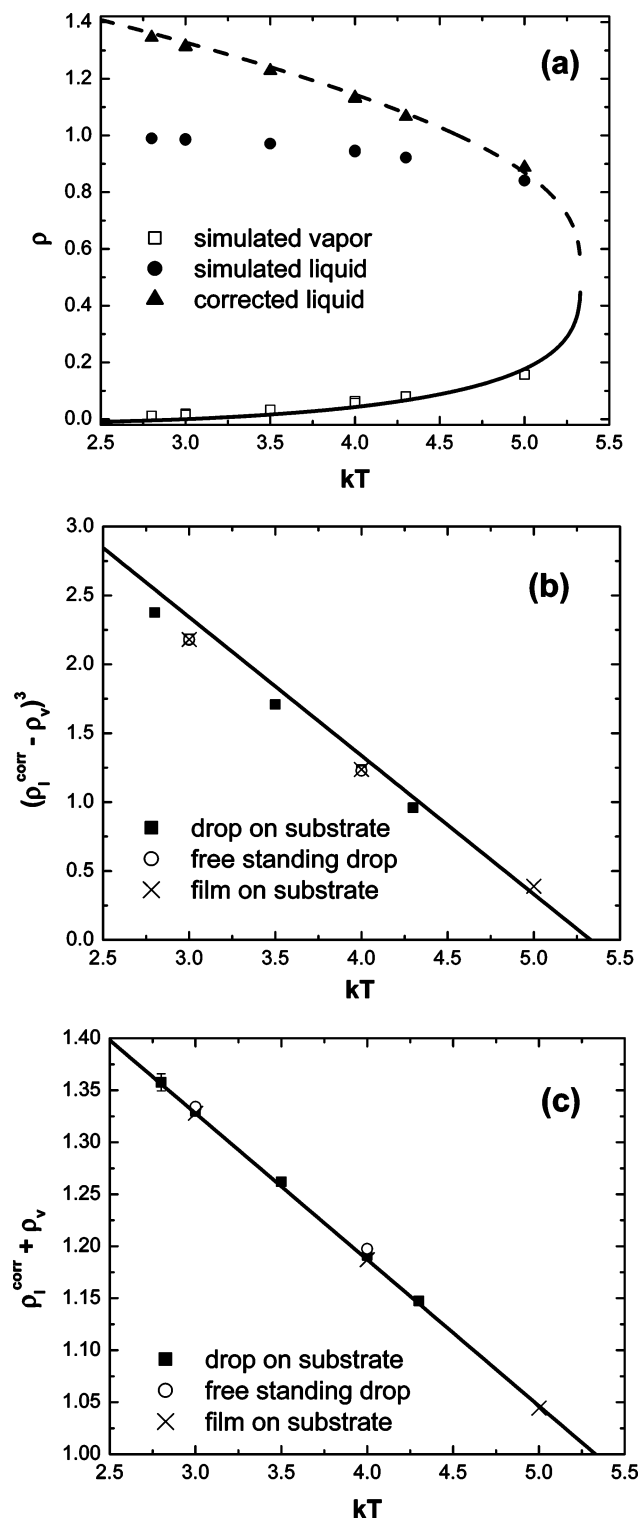
Figure 6. (a) Liquid−vapor coexistence diagram obtained from simulations. Simulated liquid densities (●) are corrected for thermal expansion (▲) as described in Appendix 1. Full line represents the fitting of vapor density according to eq 5, with the parameters $\rho_c = 0.5$ and $kT_c = 5.33 \pm 0.03$. Dashed line is the empirical curve for liquid density constructed by substituting these parameters in eq 6. (b,c) Comparison between the behavior of simulated systems and empirical laws. Full lines were built by substituting the parameters above in eqs 7 and 8 in parts b and c, respectively. When not indicated, error bars are smaller than the size of the points.

system, ξ the energy density, and V the volume. To estimate A and V, the equimolar dividing surface R_e obtained from the fitting of the density profiles was considered as the boundary
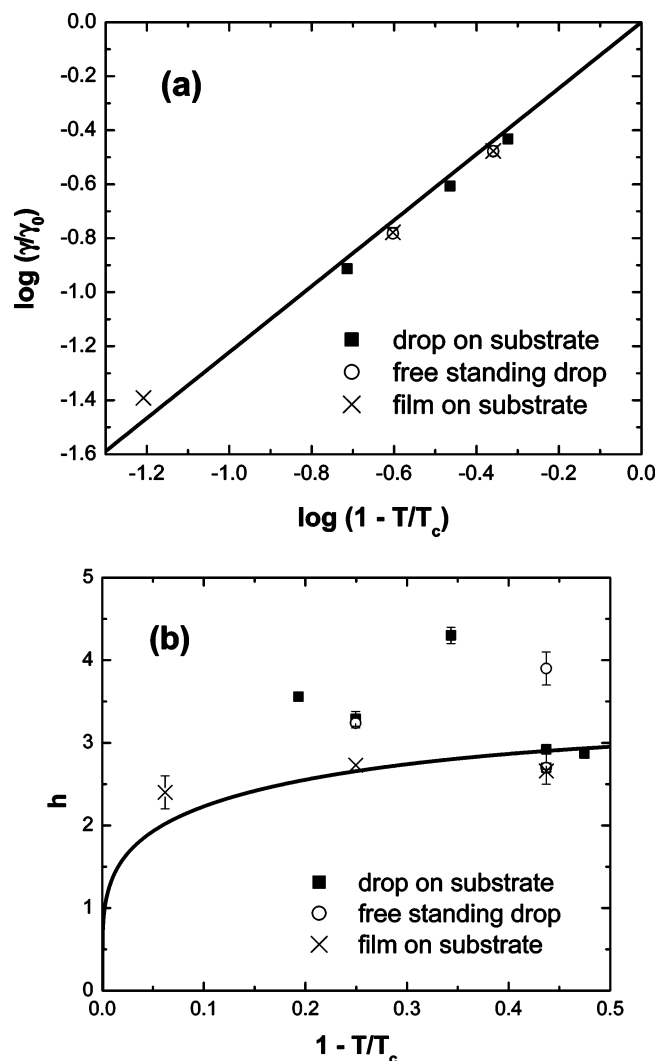

Figure 7. (a) Temperature dependence of γ/γ_0 for the simulated droplets. The straight line is the behavior expected from eq 9. (b) Temperature dependence of surface enthalpy h. The best fitting of the surface enthalpy was obtained by considering the adjustable parameter $\gamma_0 = 3.1 \pm 0.2$. Only films on substrate were taken into account in this fitting because their surface area (used in the calculation of h) can be determined more precisely. Error Bars were estimated based on the uncertainty of energy densities.
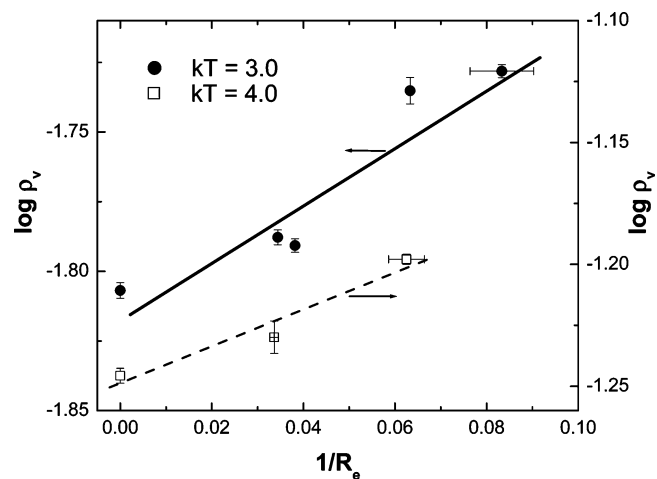

Figure 8. Variation of the vapor density as function of droplet equi-molar radius. Straight lines represent the fittings based on the Kelvin−Laplace equation.

between two phases. In Figure 7b, the calculated values are compared to the expected behavior of surface enthalpy given
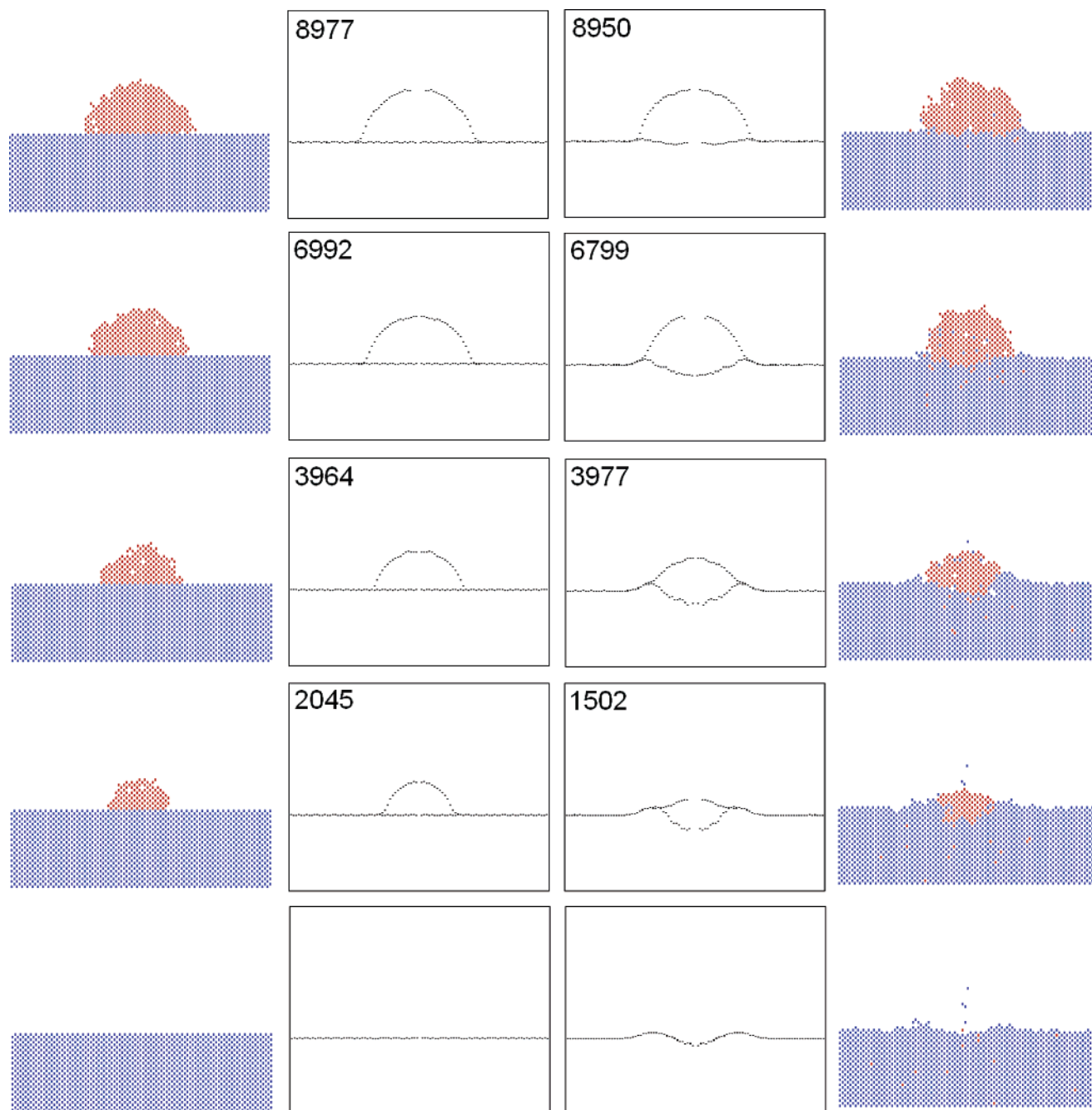
Modeling of Evaporating Droplets at Surfaces

J. Phys. Chem. B, Vol. 109, No. 9, 2005 **4157**

Figure 9. Snapshots of evaporating droplets in nonsoluble (left) and soluble (right) substrates. The white boxes are the radial average of the snapshots (the droplet center of mass was considered the center of symmetry). The number in the top of each box is the number of solvent beads remaining within the droplet.

by substituting eq 9 in the Gibbs−Helmholtz relation

$$h = \gamma - T\frac{\partial \gamma}{\partial T} \qquad (11)$$

The results shown here demonstrate that, despite the simplicity of the model, the behavior of simulated droplets agrees quite well with the experimental behavior of bulk liquids. However, a brief digression is necessary at this point. In principle, one should not compare properties of small droplets with those of bulk liquids. The vapor pressure and consequently the vapor density are higher in the case of small droplets if compared to bulk liquids, and this is known as the Kelvin−Laplace effect. Furthermore, as droplets become even smaller, the surface tension is no longer constant but varies as function of the radius of curvature.[10]

Nevertheless, there are two reasons why one can disregard these effects and consider the droplets behaving as bulk liquids. First, simulated droplets are big enough so that the surface tension does not vary with droplet radius. Molecular dynamics studies[7] have shown that the surface tension reaches its bulk value when the number of elements in the liquid phase is higher than 2000. In our work, the number of elements in the liquid phase was about 10 000. Although the interface thickness of simulated droplets is not infinitely narrow if compared to the radius of curvature, as Table 1 and Figure 5 show, the equimolar Gibbs dividing surface is a reasonable approximation for the boundary between two phases. Obviously, such approximation is not unambiguous, and this generates the data scatter in Figure 7b.
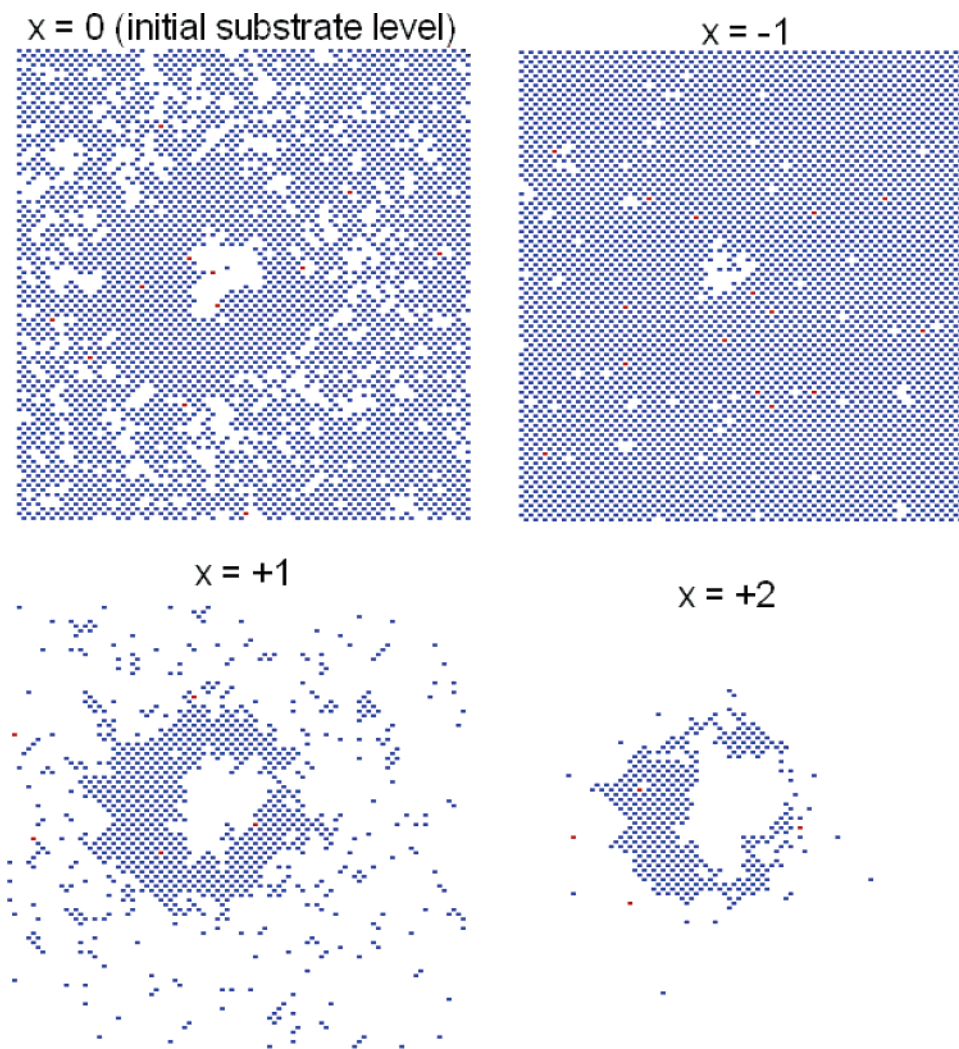
Figure 10. Snapshots of planes parallel to the substrate at several heights (*x*) showing a well surrounded by a ringlike deposit in the end of the evaporation process. Blue dots represent substrate particles.

The second point to be discussed is the influence of the Kelvin−Laplace effect on the vapor pressure. If the vapor in equilibrium with the liquid phase is regarded as an ideal gas, then this effect can be expressed as

$$P = P^{\infty} \, e^{2\gamma\bar{V}/rRT} \qquad (12)$$

where P is the pressure of vapor in equilibrium with a droplet of radius r, P^{∞} is the vapor pressure of bulk liquid, $\bar{V}$ is the molar volume of the liquid, and R is the ideal gas constant. For ideal gases, the pressure is directly proportional to the density. Figure 8 shows that the effect really takes place on simulated droplets, but the variation of the vapor density with droplet radius is very small. In fact, it will not influence significantly the value of $\rho_l - \rho_v$. This explains why droplets with different radii provide almost the same value of $\rho_l - \rho_v$. This result is very important for the next section, because it demonstrates that the simulated droplets can reproduce the behavior of droplets on the size scale of nanometers. The results can also be extended to real droplets whose size is in the range of micrometers/millimeters, where the Kelvin−Laplace effect is still insignificant.

3.2. Formation of Microwells and Ringlike Deposits. It was recently shown that if a drop of toluene of ∼300 *μ*m in diameter is placed on a polystyrene surface, then a little well surrounded by a ringlike deposit is formed as the solvent evaporates.[1] This effect is very general, i.e., it occurs for a large variety of solvents and soluble substrates. To understand it with a molecular approach, we used the droplet simulation technique explained in the last section. At this time, however, the substrate beads were allowed to move and to mix with the solvent. Another condition was that the intermixing between substrate and vacuum beads was forbidden. This was made for two reasons. First, it was made to account for the strong intermolecular bonds that should exist in solid structures and prevent the appearance of "vacuum holes" inside them. The second reason is that the incorporation of vacuum within the solid structure would change the nature of the substrate. This would add a new variable to the problem if one wants to compare these experiments with those not involving substrate swelling. Although no motion should occur inside the solid structure, substrate beads were allowed to exchange their position with other substrate beads even in the solid phase. This assumption was made to simplify the algorithm and is not unrealistic, since the identity of the beads does not change when they exchange place with each other. We believe that any solid can be regarded as an array of beads without loss of generality. Even a polymer chain could be represented by a single bead, since the simulated droplets can also scale to the micrometer size, as stated before.

The droplet evaporation was accomplished by removal of vapor. If a solvent bead mixes with vacuum and all of its

Modeling of Evaporating Droplets at Surfaces

J. Phys. Chem. B, Vol. 109, No. 9, 2005 **4159**

neighbors are vacuum beads, then the program automatically transforms it into a vacuum bead.

It turned out from the simulations that the choice of the interaction energies is crucial for microwell and ring formation. The best condition at $kT = 3.0$ was to consider the interactions SO−VA, SO−SU, and SU−VA as 1, 0.8, and 0.8, respectively. Through the use of these parameters, droplets were produced by means of relaxation of a cubic droplet. At this stage, substrate swelling was forbidden. The droplet formed this way was used in two kinds of simulations. In the first, the substrate movement was kept forbidden, but evaporation proceeded. In the second, substrate beads were allowed to move during evaporation, and a pattern in the surface was formed.

The formation of the ringlike deposit can be qualitatively deduced from the interaction values. Since the SO−SU interaction is relatively large, it is expected that the substrate will dissolve very slowly. Once they are in the liquid phase, substrate beads will migrate to the boundary between solvent and vacuum. This happens because the repulsive interaction between a dissolved substrate and vacuum is lower than that of SO−VA. The shape of the substrate surface would not change if solvent was not present because exchanges between substrate and vacuum are forbidden due to the solid structure. A solvent is necessary to swell this solid, and a structured surface is generated to minimize the energy of the system.

Figure 9 compares snapshots of the simulated system in the case of simple evaporation and substrate swelling together with evaporation. In the latter situation, the substrate is slowly dissolved by the solvent, and at the same time some solvent beads penetrate the substrate solid structure. The dissolved substrate migrates to the border of the droplet, where it forms a deposit. The result of this process is the formation of a well surrounded by a ring in the surface, as shown in Figure 10. At the end of the simulation, it can be seen that some substrate beads remain suspended in the vacuum forming a kind of "substrate gas" (Figure 9). Naturally, it is not realistic. This effect occurs because, for the sake of algorithmic simplicity, substrate beads are not allowed to exchange place with vacuum. Thus, as the solvent evaporates, some dissolved substrate beads are left away in a vacuum, where they remain immobile. One could eliminate this effect by adding gravity in the model, for example. However, the quantity of "substrate gas" corresponds only to 20% of the volume required to fill the hole.

The evaporation dynamics is intrinsically related to the formation of ringlike deposits. According to the literature, droplets can follow two evaporation schemes.[12] In the first, the contact radius decreases as the droplet evaporates, but the contact angle remains the same. In the second case, the contact radius remains constant, but the contact angle decreases (Figure 2). This effect is known as the "pinning of contact area" and occurs due to roughness or chemical inhomogeneities in the surface.[13] Previous works report that ringlike deposits occur only when the droplet contact area is pinned. It is not clear, however, if the droplet pinning is a requirement for deposit formation or rather a consequence of material deposition in the first stages of evaporation.[1,3,4]

Figure 11 compares how the shapes of simulated droplets change with time for two situations, namely, the droplet evaporation at insoluble substrate and the evaporation together with substrate swelling. In the first case, since the substrate is perfectly smooth and homogeneous, the evaporation follows the constant contact angle regime. When substrate is allowed to dissolve, the evaporation also follows this regime at early times. However, as the ring deposition starts, the contact diameter
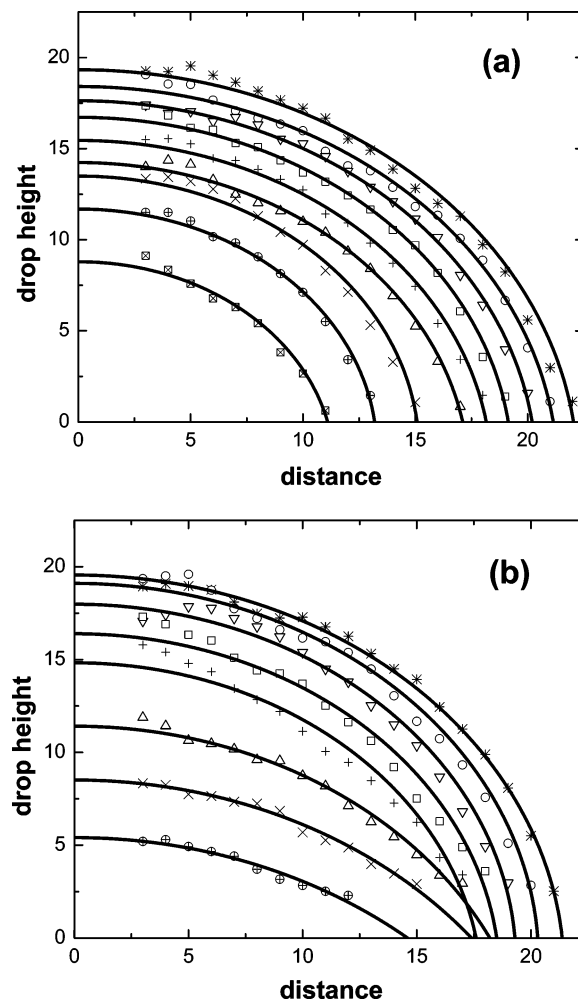

Figure 11. Average droplet shape for evaporating droplets on (a) nonsoluble and (b) soluble substrates. Full lines are mathematical fittings with the spherical cap equation.

becomes constant, and the contact angle starts to decrease, i.e., the droplet is pinned. Figure 12 shows a quantitative picture of this effect. The contact diameter and angle obtained for the case of ring formation are just apparent quantities obtained from the fitting, since the droplet does not really touch the surface at its original level because of the ring formation (Figure 13).

Our simulations support the hypothesis that the pinning of the contact area is an outcome of the solid material deposition. Pinning will occur independently of the surface roughness or its chemical identity, provided that the deposition is not hindered by this substrate.

4. Conclusions

We show that droplets on surfaces can be realistically simulated with the cooperative motion algorithm (CMA). These droplets behave like real droplets on the scale of nanometers, but the results can be extended to larger droplets with micrometer/millimeter size. The densities of the coexistent liquid and vapor phases obey empirical relations such as $\rho_l - \rho_v \propto (1 - T/T_c)^{1/3}$. In the case of soluble surfaces, it is possible to simulate the effect of microwell and ringlike deposit formation by properly choosing the interaction parameters between the components of the system. The dissolved substrate particles migrate to the border of the droplet to minimize the contact between solvent and vacuum, which costs the most energy. It is shown that the ring formation in the first stages of evaporation
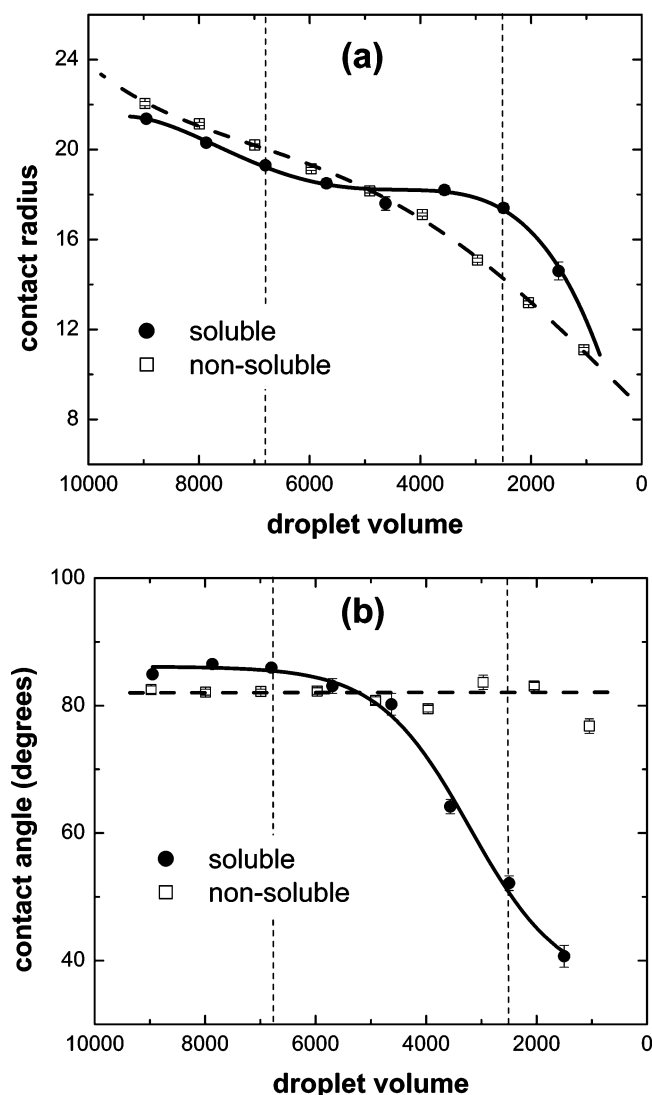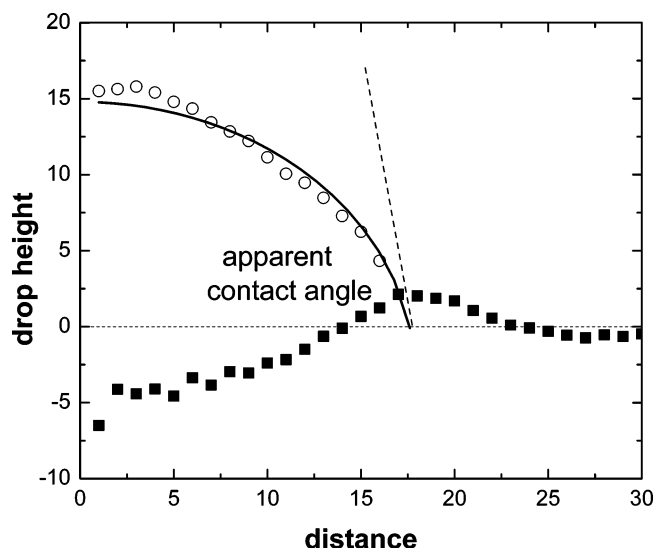
Figure 13. Determination of the apparent contact angle in the case of droplets on soluble substrates. The full line represents a spherical cap fitting.

Figure 12. Variation of (a) contact radius and (b) contact angle during evaporation. The droplet volume is regarded as the total number of solvent beads remaining in the droplet. The central region limited by the vertical dashed lines corresponds to the pinned contact area evaporation regime in the case of the soluble substrate. The thicker lines are visual guides.

results in pinning of the droplet contact area. We believe that the knowledge of these features is of relevance for the technological application of droplets in surface microstructuring.

Appendix 1. Correction of the Density of the Liquid Phase

According to the Eyring–Cremer model of liquids,[14] the volume corresponding to thermal vibrations of molecules in the liquid increases as function of temperature, causing its density to decrease. In addition to that, "holes" or "vacancies" appear inside the liquid structure at temperatures close to the critical point. Thus, the density of the liquid can be expressed as

$$\rho_l = (\rho_l^0 - aT) - \rho_{holes} \tag{13}$$

where ρ_l^0 is the liquid density at 0 K, a is its coefficient of thermal expansion, and ρ_{holes} is the density (in this case molar fraction) of holes in the liquid. The term in brackets is related to the thermal expansion of the liquid and is not reproduced by simulation methods based on a rigid lattice structure of hard spheres, but it can be considered in the lattice models by means of additional assumptions.[15] In fact, the simulation method in the version described here accounts only for the second term ρ_{holes}, since some vacuum beads manage to penetrate the liquid phase and create vacancies. Therefore, the term in brackets is the key for the correction of the liquid-phase densities obtained from simulation.

Since the Eyring–Cremer model assumes that the concentration of holes in the liquid is equal to the concentration of molecules in the vapor phase, eq 13 can be rewritten as

$$\rho_l + \rho_v = (\rho_l^0 - aT) \tag{14}$$

Through the use of eq 8 to calculate the density of the liquid at 0 K, one finds that $\rho_l^0 = 7\rho_c/2$. Through the use of this identity and substituting eq 14 in eq 8, the coefficient of thermal expansion of the liquid can be expressed as

$$a = \frac{3}{4T_c} \tag{15}$$

We will choose the critical point as a reference, and all other points will be corrected in relation to it. In this case, the expression for the corrected liquid density is given by

$$\rho_l^{corr} = \rho_l - a(T - T_c) \tag{16}$$

which becomes

$$\rho_l^{corr} = \rho_l + \frac{3}{4}\left(1 - \frac{T}{T_c}\right) \tag{17}$$

References and Notes

(1) Stupperich-Sequeira, C.; Graf, K.; Wiechert, W. Conference Proceedings 4th Mathmod. In *ARGESIM Reports*; Troch, I., Breitenecker, F., Eds.; ARGESIM-Verlag: Vienna, 2003.

(2) Gonuguntla, M.; Sharma, A. *Langmuir* **2004**, *20*, 3456–3463.

Modeling of Evaporating Droplets at Surfaces

J. Phys. Chem. B, Vol. 109, No. 9, 2005 **4161**

(3) Deegan, R. D.; Bakajin, O.; Dupont, T. F.; Huber, G.; Nagel, S. R.; Witten, T. A. *Nature* **1997**, *389*, 827−829.

(4) Deegan, R. D.; Bakajin, O.; Dupont, T. F.; Huber, G.; Nagel, S. R.; Witten, T. A. *Phys. Rev. E* **2000**, *62*, 756−765.

(5) Pakula, T. Simulations on the Completely Occupied Lattice. In *Simulation Methods for Polymers*; Kotelyanskii, M., Theodorou, D. N., Eds.; Marcel Dekker: New York, 2004; pp 147−176.

(6) Gauger, A.; Weyersberg, A.; Pakula, T. *Makromol. Chem., Theory Simul.* **1993**, *2*, 531−560.

(7) Thompson, S. M.; Gubbins, K. E.; Walton, J. P. R. B.; Chantry, R. A. R.; Rowlinson, J. S. *J. Chem. Phys.* **1984**, *81*, 530−542.

(8) Rowlinson, J. S.; Widom, B. In *Molecular Theory of Capilarity*; Baldwin, J. E., Goodenough, J. B., Halpern, J., Rowlinson, J. S., Eds.; Clarendon: Oxford, 1984; pp 173−189.

(9) Guggenheim, E. A. *J. Chem. Phys.* **1945**, *13*, 253−261.

(10) Guggenheim, E. A. *Thermodynamics, An Advanced Treatment for Chemists and Physicists*; North-Holland: Amsterdam, 1985.

(11) Zollweg, J.; Hawkins, G.; Benedek, G. B. *Phys. Rev. Lett.* **1971**, *27*, 1182−1185.

(12) Jia, W.; Qiu, H. *Int. J. Heat Mass Trans.* **2002**, *45*, 4141−4150.

(13) Butt, H.-J.; Graf, K.; Kappl, M. *Physics and Chemistry of Interfaces*; Wiley-VCH: Weinheim, 2003; pp 126−133.

(14) Luck, W. A. P. How to Understand Liquids? In *Intermolecular Forces, An Introduction to Modern Methods and Results*; Huyskens, P. L., Luck, W. A. P., Zeegers-Huyskens, T., Eds.; Springer-Verlag: Berlin, Heidelberg, 1991; pp 55−78.

(15) Pakula, T. *J. Mol. Liquids* **2000**, *86*, 109−121